JACS
JOURNAL OF THE AMERICAN CHEMICAL SOCIETY
Article
pubs.acs.org/JACS

Mixed Monolayers of Spiropyrans Maximize Tunneling Conductance Switching by Photoisomerization at the Molecule–Electrode Interface in EGaIn Junctions

Sumit Kumar,[†] Jochem T. van Herpt,[†,‡] Régis Y. N. Gengler,[†] Ben L. Feringa,[†,‡] Petra Rudolf,*[,†] and Ryan C. Chiechi*[,†,‡]

[†]Zernike Institute for Advanced Materials, Nijenborgh 4, 9747 AG Groningen, The Netherlands
[‡]Stratingh Institute for Chemistry, University of Groningen, Nijenborgh 4, 9747 AG Groningen, The Netherlands

Supporting Information

ABSTRACT: This paper describes the photoinduced switching of conductance in tunneling junctions comprising self-assembled monolayers of a spiropyran moiety using eutectic Ga–In top contacts. Despite separation of the spiropyran unit from the electrode by a long alkyl ester chain, we observe an increase in the current density J of a factor of 35 at 1 V when the closed form is irradiated with UV light to induce the ring-opening reaction, one of the highest switching ratios reported for junctions incorporating self-assembled monolayers. The magnitude of switching of hexanethiol mixed monolayers was higher than that of pure spiropyran monolayers. The first switching event recovers 100% of the initial value of J and in the mixed-monolayers subsequent dampening is not the result of degradation of the monolayer. The observation of increased conductivity is supported by zero-bias DFT calculations showing a change in the localization of the density of states near the Fermi level as well as by simulated transmission spectra revealing positive resonances that broaden and shift toward the Fermi level in the open form.

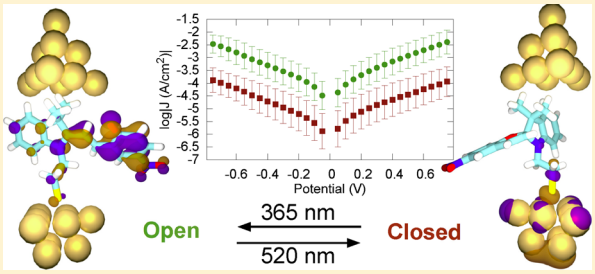

INTRODUCTION

There are two complementary goals in the study of charge transport in molecular junctions: understanding the underlying physical phenomena and extracting useful functionality, i.e., constructing devices. Break-junctions and other methods for capturing single molecules between electrodes are powerful tools for studying the physics of tunneling transport,[1] but they are limited either to sampling molecules from a population via the formation of transient junctions or proof-of-principle studies on short-lived and low-yielding devices.[2] Bottom-up tools, in which the smallest dimensions of a device are defined by the molecules in a junction,[3,4] are better suited for investigating functionality because they are long-lived (physically stable) and yield a high number of working devices.[5−7] Eutectic Ga–In (EGaIn) has proven to be a useful tool for investigating bottom-up junctions[8] to understand structure–property relationships,[9−17] to construct devices,[18] and to produce useful functionality.[19,20] However, thus far the functionality has been limited to passive properties of molecules in a self-assembled monolayer (SAM). In this work, we demonstrate control over the conductance of EGaIn/Ga_2O_3//SAM/Au^{TS} junctions with light (where "//" denotes an interface involving physisorptive bonds, "/" denotes an interface involving chemisorptive bonds, and Au^{TS} refers to template-stripped[21] Au). Junctions comprising SAMs of a spiropyran moiety (**SP**) were irradiated with either broadband visible (>520 nm) or monochromatic UV (365 nm) light to convert **SP** between the "open" merocyanine (**SP**-open) and "closed" spiropyran (**SP**-closed) forms shown in Figure 1.

The photochemical switching of **SP** on Au surfaces has been investigated in detail; it is robust and reversible.[22] Importantly,

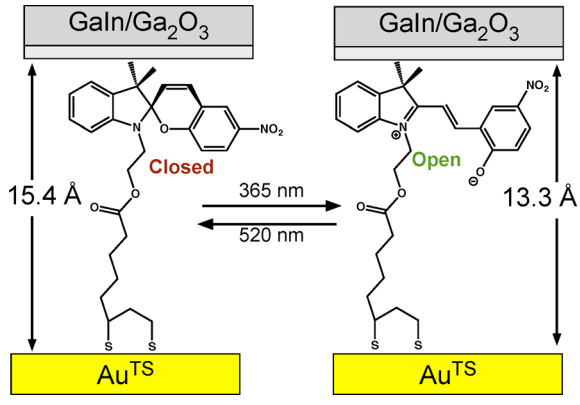

Figure 1. Schematic of the SAMs of **SP** in EGaIn/Ga_2O_3//SAM/Au^{TS} junctions in their open and closed forms. The distances are from DFT-minimized structures (the exact orientation with respect to the substrate is not known). The thickness of SAMs of the closed (left) form estimated by XPS is 15.4 ± 2 Å.

Received: July 1, 2016
Published: September 7, 2016

DOI: 10.1021/jacs.6b06806
J. Am. Chem. Soc. 2016, 138, 12519–12526

the electrochemical-induced switching is well-characterized as an irreversible dimerization pathway that can compete with reversible switching,[23] which allows us to exclude these phenomena as possible sources of conductance switching using X-ray photoelectron spectroscopy (XPS). Ring-opening of the spiropyran form (**SP**-closed) to the zwitterionic, merocyanine form (**SP**-open) is typically accomplished by irradiation with UV light. This form will revert back to **SP** spontaneously, but it is accelerated by irradiation with visible light.

Conductance switching, in which the conductance of molecules spanning two electrodes is modulated by (photo)-chemically converting molecules in-place, has been shown, for example, using azobenzenes with Hg top-contacts,[24] diaryl-ethanes with PEDOT:PSS top-contacts,[25] dihydroazulenes using reduced graphene oxide top-contacts,[26] azobenzenes covalently attached to graphene,[27] and conjugated oligomers covalently attached to carbon nanotubes.[28] Due to the lengths of the molecules involved, transport in the latter two systems is probably not dominated by tunneling, making them difficult to compare to our work. The other systems rely either on a change in tunneling distance (i.e., the *cis*/*trans* isomerization of azobenzene units) or a change in conjugation patterns (i.e., the rearrangement of bonds). The switching of **SP** induces a change in the conjugation pattern and the distribution of charge but causes a negligible change in tunneling distance (approximately 2 Å). The long aliphatic chain is what sets **SP** apart; in the aforementioned systems, the π-system is directly coupled to both electrodes, making them sensitive to small perturbations in the π-framework. The electronic structure of **SP** is more similar to those of bipyridyl- and ferrocene-terminated alkanethiols,[20,29] in which the conjugated portion is confined to the EGaIn interface and separated from the bottom electrode by a σ framework constituting a large tunneling barrier. Thus, the effects of switching **SP** are confined to the EGaIn interface (which is insensitive to a wide array of functional groups)[30,31] and are, in the absence of a pronounced change in distance, expected to be either very subtle or nonexistent; rigorous characterization of the switching process is particularly important.

A common problem to virtually all molecular junctions is that characterization is limited to the ex situ investigation of the chemical compounds, SAMs, and gaps; interrogating molecules either in situ or post factum is hindered by the small dimensions and quantities of compounds participating in transport. The rheological properties of EGaIn[32] enable both the facile formation and disassembly of junctions, allowing the interrogation of a SAM before and after both switching and applying a bias. This trait is particularly important for the study of conductance switching because virtually all switches (including **SP**) show fatigue after only a few switching cycles.[33] The reasons for this fatigue can be ascribed to desorption,[34] disorder,[35] and side reactions,[36] but only by disassembling a junction and interrogating the SAM spectroscopically can we experimentally rule out these specific effects.

RESULTS AND DISCUSSION

Formation of Self-Assembled Monolayers. We initially based the conditions for the formation of SAMs of **SP** on previous studies on roughened Au and Au-on-mica that used 10^{-4} M solutions in CH_2Cl_2.[22] However, Au^{TS} substrates do not tolerate CH_2Cl_2 because it swells the optical adhesive backing. Fortunately, **SP** is sufficiently soluble in EtOH to allow the formation of dense SAMs from 10^{-4} M solutions. Junctions comprising these SAMs were robust enough to produce current density versus voltage (J/V) data and to show conductance switching; however, the XPS data revealed unbound or physisorbed sulfur, in addition to the desired covalent Au−S species, indicating that not all of the disulfide (or thiolate) groups are attached to the Au substrate. Thus, we formed SAMs from 10^{-5} M solutions, significantly reducing the unbound/physisorbed sulfur signal and producing more robust junctions (i.e., fewer shorts). Junctions comprising these SAMs were about a factor of 10 less conductive (at 0.5 V) than those formed from 10^{-4} M solutions, but the ratio of J between **SP**-open and **SP**-closed was nearly identical. The area of the nitrogen 1s peak in the XPS data also did not differ between the two SAMs, suggesting that the difference in J is unrelated to the densities of the SAMs and may simply be a reflection of the better coupling of covalently bound sulfur, an interesting proposition given the insensitivity of EGaIn junctions to the identity of anchoring groups.[31,37,38] The XPS and J/V data for SAMs formed on Au^{TS} at 10^{-4} M are shown in the Supporting Information. Unless otherwise mentioned, all data are for SAMs formed from 10^{-5} M solutions of **SP**-closed in EtOH.

Conductance Switching. Tunneling junctions formed by making contact to a large (compared to the size of a molecule) area of a SAM, rely on statistical analyses to characterize effects because small variations in the SAM (i.e., defects) have an exponential influence on the magnitude of J, leading to data that are distributed log-normal.[11,39] This approach is particularly important for conductance switching in SAMs because the observable is often a change in J that is comparable to the junction-to-junction variation[26] due to incomplete photochemical conversion when confined to a surface.[25] There are systems that show cooperative switching (which (partially) mitigates this problem); however, they are the exception.[40] While cooperative switching can lead to changes in J of a factor of 25,[24] from the quantitative analysis of XPS spectra, we estimate the percentage of switching to **SP**-open from SAMs of **SP**-closed to be 38% and therefore expect smaller changes irrespective of the mechanism. To measure the effect of photochemically switching **SP** from the closed to open states on tunneling transport, we grew SAMs of **SP**-closed on Au^{TS} substrates and then measured the conductance through the SAMs by contacting them in various locations with tips of EGaIn and sweeping the potential from −1.0 to 1.0 V to produce a histogram of log $|J|$ for each value of V comprising data from at least 40 junctions across at least three substrates. We then irradiated each substrate with 365 nm light for 30 min immediately before performing another conductance measurement.

It is known that the roughness of the electrode supporting a SAM can strongly influence the J/V characteristics.[41,42] Of particular relevance to **SP** is the sensitivity of the packing of relatively bulky head-groups in alkane-based SAMs.[16] The driving force to form a complete thiolate monolayer competes with favorable packing of the spiropyran moieties, leading to overcrowding of the latter and incomplete coverage of the former. This steric congestion then inhibits ring-opening in the densely packed regions of the SAMs; on roughened Au beads, there is sufficient disorder to affect complete switching in one direction but apparently not the reverse.[22] To test this hypothesis, we prepared mixed-SAMs (**SP**-mixed) by incubating SAMs of **SP** in a solution of hexanethiol for 24 h, at which

DOI: 10.1021/jacs.6b06806
J. Am. Chem. Soc. 2016, 138, 12519−12526

the magnitude of switching goes through a maximum (see Figure S7).

The switching of **SP** between the closed and open forms has been shown to be reversible for at least six cycles following a "burn-in" after the first exposure to 365 nm light by integrating the area under Raman bands associated with those forms.[22] Those SAMs were formed from CH_2Cl_2 at 10^{-4} M on roughened Au, which is not compatible with conductance measurements (and surface-enhanced Raman spectroscopy is incompatible with Au^{TS}). While subtle differences in packing may affect the reversibility of the switching process on Au^{TS} substrates, we used SAMs formed from ethanol at 10^{-4} M to recreate those conditions as closely as experimentally possible. We measured J at 0.8 V for **SP**-closed from which we calculated $\Delta\log|J|$ as the SAM was cycled between the open and closed forms by subsequent exposure to 365 and >520 nm light. These data are shown in Figure 2 (black squares). For the first open−

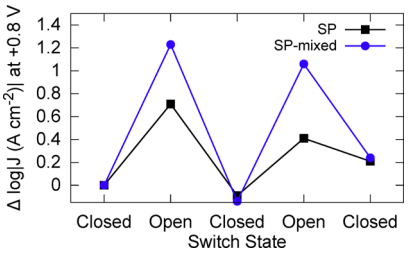

Figure 2. Plots of $\Delta\log|J|$ at 0.8 V for SAMs of **SP** (black squares) and **SP**-mixed (blue circles) on Au^{TS} as they are switched between the open and closed forms by irradiation with 365 and >520 nm light, respectively. The lines are to guide the eyes. The differences in log $|J|$ are compared to the initial measurements of **SP**-closed; thus, the negative value reflects a downward trend in conductivity of both **SP** and **SP**-mixed after the first cycle in addition to the gradual loss of the conductance switching effect (i.e., fatigue)..

closed cycle, $\Delta\log|J| \approx 0.8$ recovers completely, but the overall conductance decreases and then rapidly dampens. By the second open−closed cycle, $\Delta\log|J| \approx 0.2$. Nonetheless, the conductance switching is demonstrably reversible. The switching of **SP**-mixed (Figure 2, blue circles) shows considerably less fatigue. While the values of $\Delta\log|J|$ for **SP** and **SP**-mixed overlap exactly in the closed form, the values for **SP**-mixed in the open form are considerably higher and show less fatigue. This result implies that synthetic modifications such as those that affect the packing of the chromophore and junction optimizations (e.g., changing the contacts)[43] may extend switching past 5−7 cycles.

To gain some insight into the differences in fatigue between **SP** and **SP**-mixed, we obtained XPS spectra of **SP**-closed for both before and after repeated switching (i.e., the first and last data points of Figure 2). These data are summarized in Figure 3. The two main peaks in the N 1s core-level region (Figure 3A,C) originate from the indoline nitrogen (at a binding energy of 399.6 eV) and the NO_2 group (405.9−406.1 eV). The area under this peak is about 30% smaller for **SP**-mixed than for **SP**. After cycling of **SP**-closed with light, a new N^+ appears at 400.8 eV (**SP**-mixed) or 401.1 eV (**SP**), corresponding to the merocyanine moiety in **SP**-open.[23] The absence of this peak in Figure 3A confirms a lack of merocyanine in the SAMs of **SP** before switching. After the switching cycles, however, this peak is prominent in **SP** but comprises only 5% of the spectrum of **SP**-mixed, indicating an incomplete return to **SP**-closed for the

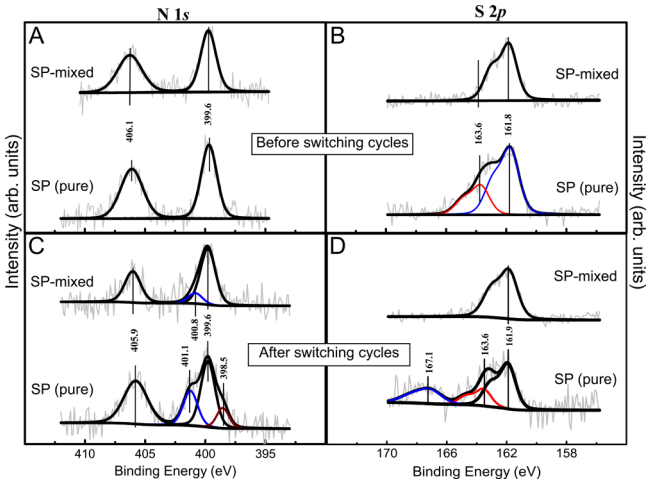

Figure 3. X-ray photoemission spectra of pristine SAMs of **SP**-closed and mixed monolayers of **SP**-closed and hexanethiol (**SP**-mixed) before and after cycling between the open and closed forms. A and B show the spectra of **SP**-closed before cycling. (A) N 1s core-level region showing no change to the nitrogen signals corresponding to the spiropyran moieties between **SP** and **SP**-mixed. (B) S 2p core-level region showing a single S−Au species in the mixed monolayer **SP**-mixed. (C and D) Same spectra after the switching cycles shown in Figure 2. (C) Spectrum of the pure SAM **SP** shows the appearance of an additional component in the N 1s core-level region at 398.5 eV that is absent in **SP**-mixed. (D) S 2p core-level region of **SP** shows an additional doublet peaked at 167.1 eV; the spectrum of **SP**-mixed is unchanged from the initial spectrum shown in the top of panel B.

pure SAMs. Figure 3B,D show the S 2p core-level region. The doublet peaked at 161.8 eV corresponds to chemisorbed **SP** (bound to the substrate through Au−S bonds).[44] The additional doublet peaked at 163.6 eV that is present only in the pure SAMs of **SP** corresponds to dimerized or physisorbed thiol,[45] indicating that not all of the **SP** molecules are attached to the substrate covalently. Thus, the hexanethiol was able to penetrate the SAM of **SP** and fill vacancies by displacing (presumably) weakly bound molecules, resulting in the exclusive formation of S−Au bonds and a complete return to **SP**-closed after the switching cycles.

The most significant difference between **SP** and **SP**-mixed after the switching cycles is the appearance of a new N 1s component at 398.5 eV in **SP**, which we ascribe to CNH_2.[46] While the other peaks, unbound thiols and residual N^+, can be attributed to structural differences in the SAMs, this peak is evidence of an unexpected side reaction causing an irreversible chemical change. The appearance of a new, more stable nitrogen species indicates that the dampening of **SP** in Figure 2 is at least partially due to damage to the SAMs of **SP** that is not present in **SP**-mixed (i.e., the component at 398.5 eV is absent in **SP**-mixed). The S 2p core-level region shows a peak at 167.1 eV for **SP** after the switching cycles (Figure 3D) corresponding to oxidized sulfur species that are completely absent in **SP**-mixed. Based on the XPS and conductivity data from cycling the switches, we suggest the following mechanism; The relatively large head-groups of the **SP** molecules lead to disordered SAMs containing a significant fraction of defects. When immersed in a solution of hexanethiol, weakly bound **SP** molecules at these defect sites are readily displaced, followed by a retarded, steady replacement of **SP** by hexanethiolate. Approximately 10 h after the retarded replacement begins, a SAM (**SP**-mixed) has formed for which the switching ratio of J

DOI: 10.1021/jacs.6b06806
J. Am. Chem. Soc. 2016, 138, 12519−12526

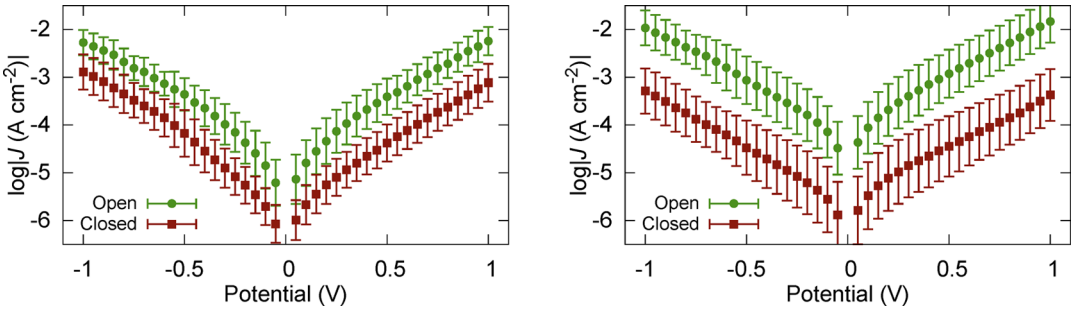

Figure 4. Current density versus voltage plots of EGaIn/Ga_2O_3//**SP**/Au^{TS} junctions in the open (green) and closed (red) forms. Left: data from pristine SAMs (**SP**). Right: data from mixed monolayers of hexanethiol and **SP** (**SP**-mixed). Each data point is the peak of a Gaussian fit of log-normal plots of |*J*| for that voltage. The error bars are the standard deviation of the Gaussian fit. The raw data are shown in the Supporting Information.

Table 1. Comparison of Switching Ratios of SP

SAM	% N^+	% N_{SP}	rel. %N^+	rel. %N_{SP}	$\frac{N^+}{N_{SP}}$	$\frac{J_{open}}{J_{closed}}$ [a]
SP-mixed	28 ± 3	22 ± 6	56	44	1.27 ± 0.35	34.5
SP	22 ± 4	36 ± 6	38	62	0.61 ± 0.14	7.4
SP[22]	19	32	37	n/d	0.59[b]	n/a

[a]From the data in Figure 4 at 1 V. [b]Calculated by us from the data in ref 22.

goes through a maximum (Figure S7). This maximum corresponds to a SAM in which the bulky head-groups are optimally packed such that they are not sterically hindered not in proximity of the metal substrate and are separated by densely packed regions of hexanethiolate, preventing side reactions and maximizing the return to the closed form after each switching cycle.

Optically switching SAMs of **SP**-mixed does not induce any (experimentally resolvable) side reactions, but there is a well-characterized electrochemical dimerization pathway for **SP**.[23,47] To show that *J*/*V* cycling with EGaIn does not induce that or any other irreversible processes, we acquired XPS data for the N 1s core-level of SAMs of **SP** before and after five sweeps at ±1 V (Figure S5). This measurement is possible because the average area of the junctions formed by EGaIn (tens of micrometers in diameter) is on the same order as that of the spot-size of the XPS instrument. Thus, we marked a region of the SAM, acquired an XPS spectrum, formed a junction, swept the voltage, and then acquired another XPS spectrum post factum. We found no change (the XPS data look identical to Figure S5) before and after the *J*/*V* sweeps. We observed no significant changes in the S 2p core-levels; the area of the doublet peaked at 163.6 eV changes by at most 1%. This result indicates both that the *J*/*V* sweeps alone do not trigger the electrochemical dimerization pathway and that the XPS does not damage the SAMs sufficiently to induce shorts. Thus, the switching between low/high conductance states and any changes present by XPS after cycling the switches can be ascribed entirely to the photochemical switching process.

We measured *J*/*V* curves for SAMs of **SP**-mixed-closed and **SP**-mixed-open under identical conditions as those used to acquire the *J*/*V* data in Figure 2. These curves are shown in Figure 4, revealing both lower values of *J* for **SP**-closed and higher values for **SP**-open. The magnitude of *J* at 1 V in SAMs of **SP** increased from $10^{-3.1}$ A cm^{-2} in the closed form to $10^{-2.2}$ A cm^{-2} in the open form, a ratio of *J* of approximately 8. The magnitude of *J* at 1 V in SAMs of **SP**-mixed increased from $10^{-3.4}$ A cm^{-2} in the closed form to $10^{-1.8}$ A cm^{-2} in the open form, a ratio of *J* of approximately 35. Together with the XPS data, these results support the hypothesis that the mixed SAM allows both for a more densely packed SAM containing the less conductive **SP**-closed form and for a more favorable packing of the spiropyran groups, leading to a higher degree of switching (to the more conductive **SP**-open). These data are summarized in Table 1. It is also possible that there is sufficient disorder in the SAMs of pure **SP** that some **SP** molecules are lying flat or folded (with unbound disulfides or physisorbed sulfur species); in either case, the mixed SAMs perform better than the pure SAMs.

Mechanism of Switching. With the phenomenon of conductance switching unambiguously established, the key question is the mechanism by which the (partial) conversion of a spiropyran moiety to its merocyanine form affects *J*. Molecules of **SP** are anchored to the surface through two thiolates attached to an ethyl octanoate linker (i.e., the equivalent of a nine-carbon alkyl chain; Figure 1); thus, the entirety of the photochemical transformation is confined to a ~3 Å layer at the EGaIn/Ga_2O_3 interface, roughly 20% of the total thickness of the monolayer. Combined with the fact that only ~38% of **SP**-closed actually switches to **SP**-open in the pure SAM, an observable change in conductance let alone an increase by a factor of 35 in **SP**-mixed is remarkable and suggests a strong effect at the molecular level. Ideally, we would establish the mechanism of charge transport as nonresonant tunneling by variable-temperature measurements, but obtaining reliable results from light-sensitive mixed-monolayers is presently unfeasible experimentally. However, the room-temperature data are perfectly symmetric, and differential conductance plots (Figure S10) are smooth and U-shaped, both of which strongly suggest nonresonant tunneling. Hopping processes arising from strong coupling to localized π-states and defects cause asymmetry[48] and negative curvature,[49] respectively.

The most obvious source of conductance switching in **SP** is a change in tunneling distance (i.e., a change in thickness of the SAM in the open and closed forms). We determined the

DOI: 10.1021/jacs.6b06806
J. Am. Chem. Soc. 2016, 138, 12519−12526

Table 2. Comparison of Shifts in Work Function, Energies of HOMOs, and V_{trans} of SP

SP SAM	HOMO (eV)[a]	ΔΦ (eV)[b]	V^{+}_{trans} (V)	V^{-}_{trans} (V)	$\mu_{\perp}$ (D)
closed	−5.20	1.0 ± 0.1	0.29 ± 0.04	−0.24 ± 0.05	8.60
open	−5.31	1.0 ± 0.1	0.25 ± 0.03	−0.23 ± 0.04	8.85

[a]Gas-phase B3LYP/TZV(2d/sp) with alkyl tails removed. [b]Measured by UPS.

thickness of SAMs of **SP**-closed to be 15.4 ± 2 Å by XPS;[50−52] however, the thickness of the SAM after switching to **SP**-open cannot be determined because the XPS signal is averaged over the spot-size and only a fraction of the molecules in the SAM switch, which would give an average height of **SP**-open and **SP**-closed. Since tunneling currents are dominated by the most conductive element of the mixed SAM,[11] the relevant value is the end-to-end length of **SP**-open. Thus, we turned to DFT calculations to help understand the changes in geometry that are associated with switching. The thicknesses shown in Figure 1 correspond to distances in the DFT optimized structures. The only geometry that corresponds to the XPS thickness of **SP**-closed is the one depicted (with the spiropyran moiety more or less parallel to the substrate), and it agrees perfectly (15.4 Å). That distance in the optimized geometry of **SP**-open is 13.3 Å, corresponding to a decrease in thickness of 2 Å upon switching with light. Any change in orientation, for example, if the merocyanine moiety rotates away from parallel, yields an increase in thickness, which would predict a lower conductance for **SP**-open. If we assume that the effect is entirely distance-dependent, then we can estimate the maximum expected change in J from the Simmons equation; $J = J_0\, e^{-\beta d}$, where $J_0 = 10^{3.4}$ A cm^{-2} and β = 0.75 Å for alkanes.[14] This estimate predicts a ratio of J of 2.0, a factor of 17.5 lower than the (maximum) experimentally observed value. For this estimate to agree with that observation, β would have to increase, meaning that SAMs of **SP** have a higher tunneling decay coefficient (β) than alkanes, which is incredibly unlikely given that $\beta \approx 0.2$ Å for π-conjugated systems.[53] It is, therefore, highly unlikely that the slight decrease in the tunneling distance is responsible for the observed increase in J in **SP**-open as compared to **SP**-closed.

Another possible mechanism of conductance switching is the change in the dipole moment perpendicular to the substrate, $\mu_{\perp}$. The collective action of $\mu_{\perp}$ in a SAM shifts the electrostatic energy (vacuum level), changing the effective work function Φ of the Au^{TS} electrode regardless of its position relative to the electrode.[54] When sufficiently close to a semiconductor interface, these dipole moments can also induce the formation of charge carriers, modulating conductivity.[55] This mechanism is unlikely because although bulk Ga_2O_3 is a semiconductor it is sufficiently thin (0.7 nm) that charges can tunnel directly to the bulk Ga−In.[56] While the effect on conductance is difficult to separate from other changes (e.g., in the orbital structure), such changes in $\mu_{\perp}$ correlate to changes in V_{trans} (the minimum of plots of $\ln[J\,V^{-2}]$ vs V^{-1}).[12,57] Thus, by comparing V_{trans} in **SP**-open and **SP**-closed, we can at least determine if the transport properties are sensitive to the difference in $\mu_{\perp}$. Table 2 summarizes the DFT-calculated HOMO energies, V_{trans} the shift in Φ with respect to bare Au^{TS} (ΔΦ) as determined from the secondary electron emission cutoff in UV photoelectron spectroscopy (UPS) data, and $\mu_{\perp}$. Surprisingly, despite the formation of a zwitterion, $\mu_{\perp}$ changes by only 0.25 D. In theory, that will induce a shift in V_{trans} of the same magnitude as the commensurate shift in vacuum level, but in practice, the value is influenced by the offset of the Fermi level of Au and the energy of the HOMO of **SP**.[58] The data are consistent; $\Delta\Delta\Phi \approx \Delta V_{trans} \approx 0$. There is almost no difference in Φ before and after switching. Although there is a shift in $V^{+}_{trans} \approx 0.3$ eV (and a calculated shift in the HOMO of approximately 0.1 eV), the values are within one standard deviation, and there is no change to V^{-}_{trans} (Figure S2). We can conclude only that the change in $\mu_{\perp}$ has either little or no effect on V_{trans} and therefore likely no effect on J.

The changes in tunneling distance and $\mu_{\perp}$ are probably too subtle to explain the relatively large change in log |J| that accompanies switching between **SP**-open and **SP**-closed. The last parameter likely to have an influence on conductance is the distribution and relative energies of the density of states (DOS) near the energy of the Fermi level, E_f. Figure 5A is a schematic of a model junction comprising the spiropyran and merocyanine portions of single molecules of **SP** including DFT-minimized geometries and the spatial distribution of the

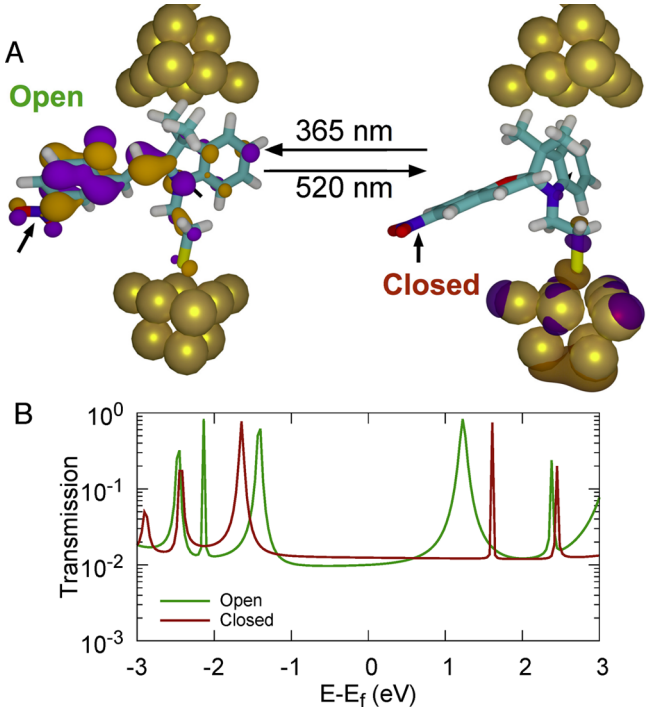

Figure 5. A: A schematic of a model junction comprising the optimized geometry of the **SP** fragment that would be in contact with the EGaIn electrode and the distribution of the DOS derived from the vacuum HOMO of **SP**-open (left) and **SP**-closed (right). The two nitrogen atoms in each isomer are indicated with arrows for clarity. The DOS is localized on the electrode for **SP**-closed, but spans the entire junction for **SP**-open. B: Simulated transmission curves of the model junctions at zero bias with E_f set to −4.5 eV. The x-axis is the energy offset of the molecular states with respect to E_f and is not related to the experimental applied bias. The shift in electron density is reflected in these curves, which show resonances shifting closer to the center of the bias window. This effect is particularly evident around 1.0 eV, where a broad resonance appears for **SP**-open.

DOI: 10.1021/jacs.6b06806
J. Am. Chem. Soc. 2016, 138, 12519−12526

DOS derived from the vacuum HOMO. The alkyl anchors were truncated to two carbon atoms to simulate the isolation of the spiropyran moiety from the thiol without having to minimize the entire alkyl chain. The DOS that is localized to the bottom electrode (i.e.,the S−Au contact) in **SP**-closed delocalizes across the molecule in **SP**-open. While there are deeper orbitals in **SP**-closed that do span the electrode, transport is dominated by the orbitals nearest in energy to E_f. A similar situation occurring very near resonance manifests as rectification[59,60] rather than ΔJ, but the principle is the same: Delocalized states near E_f affect the rate of tunneling.

These calculations are not models of an EGaIn junction, which would have to include the (unknown) details of the SAM//Ga_2O_3 interface, the packing of **SP** (and **SP**-mixed) on Au^{TS}, and the broadening and electrostatic effects of the SAM on the level alignment. Rather, they are model junctions showing the zero-bias transmission spectra of single molecules between clusters of Au meant to examine electronic effects intrinsic to the structure of **SP**-open and **SP**-closed; it is reasonable to assume these effects would manifest in the commensurate Au^{TS}/SAM//EGaIn junction. A qualitative description of the switching mechanism based on these electronic effects can be thought of as a molecular analog of a mercury switch; in the open form, the *p*-nitrophenol moiety rotates, becoming coplanar with the indoline moiety and molecular orbitals spread (like mercury flowing in a switch) to the electrode interface, "closing the contact" and increasing the total conductance. The plot in Figure 5B is a more quantitative description, showing simulated zero-bias transmission curves for **SP**-open and **SP**-closed. We set E_f to −4.5 eV, which is approximately the average of Ga, In, and Au. (This choice is somewhat arbitrary as the plots would not change if referenced to the vacuum level since both junctions have the same molecular formula.) As is depicted in Figure 5A, we approximate the electrodes with 9- or 10-atom clusters of Au. These curves show the qualitative description of the switching effect in detail; **SP**-closed shows two sharp resonances more than 1.5 eV above/below E_f. In **SP**-open, these peaks broaden and shift closer to E_f and into the bias window, particularly above E_f where a broad resonance dips below 1.0 eV. Given the noncovalent EGaIn/**SP** interface and the long alkyl spacer at the Au electrode, it is reasonable to assume[61] that regardless of the true value of E_f the Fermi level lies in the frontier orbital gap of **SP** and that the transmission calculation predicts that one or both frontier orbitals will shift toward it and broaden. Thus, **SP**-open will likely exhibit higher values of J than **SP**-closed under bias. While we cannot know for certain what effect an applied bias will have on the transmission features in a real EGaIn junction, the movement of the resonant peaks closer to E_f and within the range of applied bias supports the experimental observation that **SP**-open is more conductive than **SP**-closed. We used a similar analysis to describe a photogating effect by considering the effective change in distance when DOS appears on a chromophore attached to an alkyl tail under irradiation.[43] Using that same analysis, **SP** falls exactly on a trendline of percentage change in effective distance (29.3%) versus ratio of J (Figure S6), further supporting the "mercury switch" mechanism described above.

CONCLUSIONS

While the general phenomenon of photoisomerization leading to a change in tunneling currents is relatively well-known, examples of switching in-place (as opposed to sampling from a population) are mostly limited to diazobenzene, dyhydroazulene, and diarylethene moieties.[24−27,62] Distance effects are based on the *cis*/*trans* isomerization of diazobenzene comprising some fraction of an alkane-based SAM, and the mechanism is easily understood. Switching based on the rearrangement of bonds is mainly confined to π-conjugated molecules spanning electrodes, and the mechanisms are not typically elucidated beyond very general concerns such as differing conjugation patterns. Switching ratios are typically on the order of 5−25. We have demonstrated conductance switching based on the photoisomerization of spiropyran moieties supported by long alkyl chains that is not accompanied by an appreciable change in distance. We observed an increase in the magnitude of conductance switching from a factor of 8 in pristine SAMs to 35 in mixed SAMs, accompanied by a decrease in fatigue with repeated switching. We ascribe the superior performance of the mixed SAMs to optimized packing of the spiropyrans at the electrode interface. The direction of switching (i.e., that **SP**-open is the more conductive form) is supported by DFT calculations showing that the DOS is localized on the Au^{TS} electrode in the closed form but that it delocalizes in the open form. Simulated transmission spectra confirm that this delocalization shifts positive resonances closer to E_f and broadens them, leading to higher conductivity.

An important consideration concerning phenomena in molecular electronics that are ostensibly targeted at (not very near) future applications is that the observations in static devices that do not damage the molecules under investigation. In this study, the first switching event is completely reversible, followed by a dampening that is not the result of electrochemical degradation. The fact that cycling EGaIn junctions does not (substantially) damage the SAMs leaves open the possibility of further optimization. These results also provide additional evidence that simulated transmission curves on single molecules placed between clusters of Au are useful models for experimentally observed trends in large-area junctions such as those formed with EGaIn.[9]

EXPERIMENTAL SECTION

Substrate Preparation. Smooth gold surfaces (Au^{TS}) were prepared by template stripping.[21] First, 100 nm of Au on Si(100) substrates was prepared by evaporation of 99.99% Au (Schöne Edelmetaal B.V.) on the clean Si wafer (Prime wafers) at 300 K. Piranha-cleaned glass substrates of 1 cm × 1 cm were then glued (Norland 61) onto a freshly prepared Au/Si surface. The glass/Au/Si sandwich substrates were cured under UV lamp for 5 min. The smooth Au surface was prepared immediately before use by mechanically separating the glass/Au structures from the Si to expose the buried interface.

Monolayer Preparation and Handling. The synthesis and characterization of **SP** are provided in ref 22. Self-assembled monolayers of spiropyran were prepared by incubating freshly cleaved Au^{TS} surfaces in 10^{-5} or 10^{-4} M solutions of spiropyran (**SP**) in degassed ethanol overnight at room temperature in the dark. The surfaces were then rinsed with ethanol, thoroughly dried with dry Ar, and immediately introduced into the measuring system. Switching to the open form was accomplished by exposing the SAMs to UV (365 nm) light for 30 min using a 365 nm (central wavelength). Spectroline spectrometer (model no. ENB280C/FE) lamp. Mixed monolayers of hexanethiol and **SP** were prepared by immersing a freshly cleaved Au^{TS} substrate in a 10^{-4} M solution of **SP** in ethanol for 10 min and then in a 10^{-2} M solution of hexanethiol in ethanol for 24 h. Monolayer preparation was carried out under an inert atmosphere in degassed solvents, in a dark room, and at room temperature. All transport measurements were carried out in a reduced O_2 environment (1−3%)

DOI: 10.1021/jacs.6b06806
J. Am. Chem. Soc. 2016, 138, 12519−12526

at low (<5%) relative humidity to minimize oxidative damage to the SAMs. Tunneling junctions were formed by contacting the SAMs of **SP** on Au^{TS} surfaces with a sharp tip of EGaIn (see Supporting Information for details). Control measurements on SAMs of alkanethiolates did not exhibit any switching upon irradiation (Figure S9).

X-ray Photoelectron Spectroscopy. XPS was performed with a Surface Science SSX-100 ESCA instrument equipped with a monochromatic Al Kα X-ray source ($h\nu$ = 1486.6 eV). The measurement chamber pressure was maintained below 10^{-9} mbar during data acquisition. The electron takeoff angle with respect to the surface normal was 37°. The diameter of the analyzed area was 1000 μm; the energy resolution was set to 1.1 eV to minimize data acquisition times. XPS spectra were analyzed by using the least-squares curve fitting program Winspec (developed in the LISE laboratory of the Facultés Universitaires Notre-Dame de la Paix, Namur, Belgium). Binding energies are reported ±0.1 eV and are referenced to the Au $4f_{7/2}$ photoemission peak originating from the substrate, centered at a binding energy of 84.0 eV.[63] Deconvolution of spectra included a Shirley baseline[64] subtraction and fitting with a minimum number of peaks consistent with the structure of molecule on the surface, taking into account the experimental resolution. The profile of the peak was taken as a convolution of Gaussian and Lorentzian functions. The uncertainty in the peak intensity determination is 5% for nitrogen and sulfur and 2% for carbon, gold, and oxygen. All measurements were carried out using freshly prepared samples; five spots were measured on each surface to check for reproducibility.

UV Photoelectron Spectroscopy. To determine the change in work function of the gold surface modified by a SAM of **SP**, UPS spectra were collected using a CALM 100 spectrometer (VG Scientific Limited) with He I photons (21.1 eV, Focus VUV source NG HIS); the energy resolution was 0.1 eV. A −5.0 V bias was applied between the sample and detector to separate secondary electrons from the sample from secondary electrons generated in the analyzer. The work function[65] ($e\phi$) was determined by fitting the secondary electron cutoff with a straight line.

***J/V* Data Acquisition.** Data were acquired using a lab-built setup that is described in detail elsewhere.[9] Briefly, an EGaIn tip was formed by extruding a droplet from the barrel of a 15 μL syringe, placing it in contact with a sacrificial substrate and withdrawing it slowly. Using a micromanipulator, the syringe was lowered until the tip made visible contact with Au^{TS} surfaces supporting the SAMs of **SP**. A Keithley 6430 subfemto electrometer with an external pre-amp was used to bias the EGaIn against the Au^{TS}, which was grounded (the opposite of many probe-based conductance measurements). The setup was housed inside a flowbox that maintained a N_2 atmosphere of <5% relative humidity and 1−3% O_2. The conductance of each SAM in the open or closed form was determined by acquiring at least 420 scans in 40 different positions across 3 substrates for an average of 5 scans per junction. The bias window of ±1 V was chosen by gradually increasing the window from ±0.85 V until signs of damage from excessive short circuits or electrochemical damage became apparent (at greater than ±1 V). The raw data were processed automatically and without pruning using Scientific Python to produce histograms of log |*J*| for each value of *V* and compute V_{trans} from the Fowler−Nordheim plots ($\ln(J/V)$ vs V^2) of each *J*/*V* curve. Histograms of log |*J*| for each value of *V* and of V_{trans} are shown in the Supporting Information.

Calculations. Calculations were performed using ORCA 3.03 and ARTAIOS.[66,67] Structures were first minimized by BP/TZV(sp); then, the single-point energies were computed by B3LYP/TZV(2d/sp) using ORCA. Transmission curves were computed in ARTAIOS using outputs from B3LYP/D95(LANL2DZ) calculations based on the minimized geometries.

■ ASSOCIATED CONTENT

Supporting Information

The Supporting Information is available free of charge on the ACS Publications website at DOI: 10.1021/jacs.6b06806.

Additional XPS data, statistics, a plot of comparative changes to tunneling distance, and conductance data (PDF)

■ AUTHOR INFORMATION

Corresponding Authors

*E-mail: p.rudolf@rug.nl.

*E-mail: r.c.chiechi@rug.nl

Notes

The authors declare no competing financial interest.

■ ACKNOWLEDGMENTS

R.C.C. acknowledges the European Research Council for the ERC Starting Grant 335473 (MOLECSYNCON). S.K. acknowledges support from the Svāgata 2013 Erasmus Mundus Programme of the European Commission.

■ REFERENCES

(1) Xiang, D.; Jeong, H.; Lee, T.; Mayer, D. *Adv. Mater.* **2013**, *25*, 4845−4867.

(2) Song, H.; Kim, Y.; Jang, Y. H.; Jeong, H.; Reed, M.; Lee, T. *Nature* **2009**, *462*, 1039−1043.

(3) Simeone, F. C.; Rampi, M. A. *Chimia* **2010**, *64*, 362−369.

(4) Zhang, Y.; Zhao, Z.; Fracasso, D.; Chiechi, R. C. *Isr. J. Chem.* **2014**, *54*, 513−533.

(5) Akkerman, H. B.; Blom, P. W. M.; de Leeuw, D. M.; de Boer, B. *Nature* **2006**, *441*, 69−72.

(6) van Hal, P. A.; Smits, E. C. P.; Geuns, T. C. T.; Akkerman, H. B.; De Brito, B. C.; Perissinotto, S.; Lanzani, G.; Kronemeijer, A. J.; Geskin, V.; Cornil, J.; Blom, P. W. M.; de Boer, B.; de Leeuw, D. M. *Nat. Nanotechnol.* **2008**, *3*, 749−754.

(7) Pourhossein, P.; Chiechi, R. C. *ACS Nano* **2012**, *6*, 5566−5573.

(8) Chiechi, R. C.; Weiss, E. A.; Dickey, M. D.; Whitesides, G. M. *Angew. Chem.* **2008**, *120*, 148−150.

(9) Fracasso, D.; Valkenier, H.; Hummelen, J. C.; Solomon, G. C.; Chiechi, R. *J. Am. Chem. Soc.* **2011**, *133*, 9556−9563.

(10) Yuan, L.; Breuer, R.; Jiang, L.; Schmittel, M.; Nijhuis, C. A. *Nano Lett.* **2015**, *15*, 5506−5512.

(11) Weiss, E. A.; Chiechi, R. C.; Kaufman, G. K.; Kriebel, J. K.; Li, Z.; Duati, M.; Rampi, M. A.; Whitesides, G. M. *J. Am. Chem. Soc.* **2007**, *129*, 4336−4349.

(12) Kovalchuk, A.; Abu-Husein, T.; Fracasso, D.; Egger, D. A.; Zojer, E.; Zharnikov, M.; Terfort, A.; Chiechi, R. C. *Chem. Sci.* **2016**, *7*, 781−787.

(13) Baghbanzadeh, M.; Simeone, F. C.; Bowers, C. M.; Liao, K.-C.; Thuo, M.; Baghbanzadeh, M.; Miller, M. S.; Carmichael, T. B.; Whitesides, G. M. *J. Am. Chem. Soc.* **2014**, *136*, 16919−16925.

(14) Simeone, F. C.; Yoon, H. J.; Thuo, M. M.; Barber, J. R.; Smith, B.; Whitesides, G. M. *J. Am. Chem. Soc.* **2013**, *135*, 18131−18144.

(15) Thuo, M. M.; Reus, W. F.; Nijhuis, C. A.; Barber, J. R.; Kim, C.; Schulz, M. D.; Whitesides, G. M. *J. Am. Chem. Soc.* **2011**, *133*, 2962−2975.

(16) Nerngchamnong, N.; Yuan, L.; Qi, D.-C.; Li, J.; Thompson, D.; Nijhuis, C. A. *Nat. Nanotechnol.* **2013**, *8*, 113−8.

(17) Castañeda Ocampo, O. E. C.; Gordiichuk, P.; Catarci, S.; Gautier, D. A.; Herrmann, A.; Chiechi, R. C. *J. Am. Chem. Soc.* **2015**, *137*, 8419−8427.

(18) Wan, A.; Suchand Sangeeth, C. S. S.; Wang, L.; Yuan, L.; Jiang, L.; Nijhuis, C. A. *Nanoscale* **2015**, *7*, 19547−19556.

(19) Nijhuis, C. A.; Reus, W. F.; Siegel, A. C.; Whitesides, G. M. *J. Am. Chem. Soc.* **2011**, *133*, 15397−15411.

(20) Yoon, H. J.; Liao, K. C.; Lockett, M. R.; Kwok, S. W.; Baghbanzadeh, M.; Whitesides, G. M. *J. Am. Chem. Soc.* **2014**, *136*, 17155−17162.

(21) Weiss, E. A.; Kaufman, G. K.; Kriebel, J. K.; Li, Z.; Schalek, R.; Whitesides, G. M. *Langmuir* **2007**, *23*, 9686−9694.

(22) Ivashenko, O.; van Herpt, J. T.; Feringa, B. L.; Rudolf, P.; Browne, W. R. *Langmuir* **2013**, *29*, 4290−4297.
(23) Ivashenko, O.; van Herpt, J. T.; Feringa, B. L.; Rudolf, P.; Browne, W. R. *J. Phys. Chem. C* **2013**, *117*, 18567−18577.
(24) Ferri, V.; Elbing, M.; Pace, G.; Dickey, M. D.; Zharnikov, M.; Samorí, P.; Mayor, M.; Rampi, M. A. *Angew. Chem., Int. Ed.* **2008**, *47*, 3407−3409.
(25) Kronemeijer, A. J.; Akkerman, H. B.; Kudernac, T.; van Wees, B. J.; Feringa, B. L.; Blom, P. W. M.; de Boer, B. *Adv. Mater.* **2008**, *20*, 1467−1473.
(26) Li, T.; Jevric, M.; Hauptmann, J. R.; Hviid, R.; Wei, Z.; Wang, R.; Reeler, N. E. A.; Thyrhaug, E.; Petersen, S.; Meyer, J. A. S.; Bovet, N.; Vosch, T.; Nygård, J.; Qiu, X.; Hu, W.; Liu, Y.; Solomon, G. C.; Kjaergaard, H. G.; Bjornholm, T.; Nielsen, M. B.; Laursen, B. W.; Nørgaard, K. *Adv. Mater.* **2013**, *25*, 4164−4170.
(27) Seo, S.; Min, M.; Lee, S. M.; Lee, H. *Nat. Commun.* **2013**, *4*, 1920.
(28) Guo, X.; Small, J. P.; Klare, J. E.; Wang, Y.; Purewal, M. S.; Tam, I. W.; Hong, B. H.; Caldwell, R.; Huang, L.; O'brien, S.; Yan, J.; Breslow, R.; Wind, S. J.; Hone, J.; Kim, P.; Nuckolls, C. *Science* **2006**, *311*, 356−359.
(29) Nijhuis, C. A.; Reus, W. F.; Whitesides, G. M. *J. Am. Chem. Soc.* **2009**, *131*, 17814−17827.
(30) Yoon, H. J. H.; Shapiro, N. D. N.; Park, K. M. K.; Thuo, M. M. M.; Soh, S. S.; Whitesides, G. M. G. *Angew. Chem., Int. Ed.* **2012**, *51*, 4658−4661.
(31) Liao, K. C.; Yoon, H. J.; Bowers, C. M.; Simeone, F. C.; Whitesides, G. M. *Angew. Chem., Int. Ed.* **2014**, *53*, 3889−3893.
(32) Dickey, M. D.; Chiechi, R. C.; Larsen, R. J.; Weiss, E. A.; Weitz, D. A.; Whitesides, G. M. *Adv. Funct. Mater.* **2008**, *18*, 1097−1104.
(33) Pijper, T. C.; Ivashenko, O.; Walko, M.; Rudolf, P.; Browne, W. R.; Feringa, B. L. *J. Phys. Chem. C* **2015**, *119*, 3648−3657.
(34) Shon, Y.-S.; Lee, T. R. *J. Phys. Chem. B* **2000**, *104*, 8192−8200.
(35) Prathima, N.; Harini, M.; Rai, N.; Chandrashekara, R. H.; Ayappa, K. G.; Sampath, S.; Biswas, S. K. *Langmuir* **2005**, *21*, 2364−2374.
(36) Brewer, N. J.; Janusz, S.; Critchley, K.; Evans, S. D.; Leggett, G. J. *J. Phys. Chem. B* **2005**, *109*, 11247−11256.
(37) Fracasso, D.; Kumar, S.; Rudolf, P.; Chiechi, R. C. *RSC Adv.* **2014**, *4*, 56026−56030.
(38) Bowers, C. M.; Liao, K.-C.; Zaba, T.; Rappoport, D.; Baghbanzadeh, M.; Breiten, B.; Krzykawska, A.; Cyganik, P.; Whitesides, G. M. *ACS Nano* **2015**, *9*, 1471−1477.
(39) Reus, W. F.; Nijhuis, C. A.; Barber, J. R.; Thuo, M. M.; Tricard, S.; Whitesides, G. M. *J. Phys. Chem. C* **2012**, *116*, 6714−6733.
(40) Pace, G.; Ferri, V.; Grave, C.; Elbing, M.; von Hänisch, C.; Zharnikov, M.; Mayor, M.; Rampi, M. A.; Samorí, P. *Proc. Natl. Acad. Sci. U. S. A.* **2007**, *104*, 9937−9942.
(41) Yuan, L.; Jiang, L.; Thompson, D.; Nijhuis, C. A. *J. Am. Chem. Soc.* **2014**, *136*, 6554−6557.
(42) Chen, J.; Wang, Z.; Oyola-Reynoso, S.; Gathiaka, S. M.; Thuo, M. *Langmuir* **2015**, *31*, 7047−7054.
(43) Pourhossein, P.; Vijayaraghavan, R. K.; Meskers, S. C. J.; Chiechi, R. C. *Nat. Commun.* **2016**, *7*, 11749.
(44) Nuzzo, R. G.; Zegarski, B. R.; Dubois, L. H. *J. Am. Chem. Soc.* **1987**, *109*, 733−740.
(45) Duwez, A.-S. *J. Electron Spectrosc. Relat. Phenom.* **2004**, *134*, 97−138.
(46) Dementjev, A.; de Graaf, A.; van de Sanden, M.; Maslakov, K.; Naumkin, A.; Serov, A. *Diamond Relat. Mater.* **2000**, *9*, 1904−1907.
(47) Ivashenko, O.; van Herpt, J. T.; Rudolf, P.; Feringa, B. L.; Browne, W. R. *Chem. Commun.* **2013**, *49*, 6737−6739.
(48) Kong, G. D.; Kim, M.; Cho, S. J.; Yoon, H. J. *Angew. Chem., Int. Ed.* **2016**, *55*, 10307−10311.
(49) Jiang, L.; Sangeeth, C. S. S.; Wan, A.; Vilan, A.; Nijhuis, C. A. *J. Phys. Chem. C* **2015**, *119*, 960−969.
(50) Valkenier, H.; Huisman, E. H.; van Hal, P. A.; de Leeuw, D. M.; Chiechi, R. C.; Hummelen, J. C. *J. Am. Chem. Soc.* **2011**, *133*, 4930−4939.
(51) Thome, J.; Himmelhaus, M.; Zharnikov, M.; Grunze, M. *Langmuir* **1998**, *14*, 7435−7449.
(52) Bain, C. D.; Whitesides, G. M. *J. Phys. Chem.* **1989**, *93*, 1670−1673.
(53) Sangeeth, C. S. S.; Demissie, A. T.; Yuan, L.; Wang, T.; Frisbie, C. D.; Nijhuis, C. A. *J. Am. Chem. Soc.* **2016**, *138*, 7305−7314.
(54) Abu-Husein, T.; Schuster, S.; Egger, D. A.; Kind, M.; Santowski, T.; Wiesner, A.; Chiechi, R.; Zojer, E.; Terfort, A.; Zharnikov, M. *Adv. Funct. Mater.* **2015**, *25*, 3943−3957.
(55) Suda, M.; Kato, R.; Yamamoto, H. M. *Science* **2015**, *347*, 743−746.
(56) Cademartiri, L.; Thuo, M. M.; Nijhuis, C. A.; Reus, W. F.; Tricard, S.; Barber, J. R.; Sodhi, R. N. S.; Brodersen, P.; Kim, C.; Chiechi, R. C.; Whitesides, G. M. *J. Phys. Chem. C* **2012**, *116*, 10848−10860.
(57) Fracasso, D.; Muglali, M. I.; Rohwerder, M.; Terfort, A.; Chiechi, R. C. *J. Phys. Chem. C* **2013**, *117*, 11367−11376.
(58) Kim, B.; Choi, S. H.; Zhu, X.-Y.; Frisbie, C. D. *J. Am. Chem. Soc.* **2011**, *133*, 19864−19877.
(59) Van Dyck, C.; Ratner, M. A. *Nano Lett.* **2015**, *15*, 1577−1584.
(60) Yuan, L.; Nerngchamnong, N.; Cao, L.; Hamoudi, H.; del Barco, E.; Roemer, M.; Sriramula, R. K.; Thompson, D.; Nijhuis, C. A. *Nat. Commun.* **2015**, *6*, 6324.
(61) Paulsson, M.; Datta, S. *Phys. Rev. B: Condens. Matter Mater. Phys.* **2003**, *67*, 241403.
(62) Mativetsky, J. M.; Pace, G.; Elbing, M.; Rampi, M. A.; Mayor, M.; Samorí, P. *J. Am. Chem. Soc.* **2008**, *130*, 9192−9193.
(63) Moulder, J. F.; Stickle, W. F.; Sobol, P. E.; Bomben, K. D. *Handbook of X-Ray Photoelectron Spectroscopy*; Perkin-Elmer Corporation: Eden Prairie, MN, 1992.
(64) Shirley, D. A. *Phys. Rev. B* **1972**, *5*, 4709−4714.
(65) Helander, M.; Greiner, M.; Wang, Z.; Lu, Z. *Appl. Surf. Sci.* **2010**, *256*, 2602−2605.
(66) Herrmann, C.; Solomon, G. C.; Subotnik, J. E.; Mujica, V.; Ratner, M. A. *J. Chem. Phys.* **2010**, *132*, 024103.
(67) Neese, F. *Wiley Interdiscip. Rev.: Comput. Mol. Sci.* **2012**, *2*, 73−78.

DOI: 10.1021/jacs.6b06806
J. Am. Chem. Soc. 2016, 138, 12519−12526